Efficient band gap prediction of semiconductors and insulators from a semilocal exchange-correlation functional

Bikash Patra,[1,*] Subrata Jana,[1,†] Lucian A. Constantin,[2,‡] and Prasanjit Samal[1,§]
[1]*School of Physical Sciences, National Institute of Science Education and Research, HBNI, Bhubaneswar 752050, India*
[2]*Center for Biomolecular Nanotechnologies @UNILE, Istituto Italiano di Tecnologia, Via Barsanti, I-73010 Arnesano, Italy*

(Received 5 April 2019; revised manuscript received 14 June 2019; published 29 July 2019)

A semilocal exchange-correlation functional is proposed with the efficient prediction of the solid-state band gap. The underlying construction of the exchange functional is based on the modeling of the exchange hole and constructing the exchange energy functional. Being a meta-generalized gradient approximation (meta-GGA) level functional, it holds the key feature of the derivative discontinuity through the generalized Kohn-Sham (gKS) formalism. We validate our construction by demonstrating the functional performance for solid-state band gaps and comparing it with the other meta-GGA and hybrid functionals. It is shown that for the semiconductors having narrow, and moderate band gaps, as well as for layered materials the present functional performs as accurately as (or comparable to) the expensive hybrid functional, while for wide-band gap solids, it outperforms the hybrid functional. This indicates that the present functional holds promise for the multiscale modeling of materials with a very low computational cost. Also, the underlying construction is practically very useful as it can be easily implemented in any density functional platform that supports the gKS formalism.

DOI: 10.1103/PhysRevB.100.045147

I. INTRODUCTION

The Kohn-Sham (KS) [1,2] formalism of the density functional theory (DFT) is the *de facto* standard method to account for the electronic structure calculations of the atoms, molecules, solids, and materials. In KS-DFT, the central task is to construct the exchange-correlation (XC) energy functional or potential. Starting from the local-density approximation (LDA) [2], the higher rungs of the semilocal XC functionals are represented by the generalized gradient approximation (GGAs) [3–27], and meta-GGAs [28–43]. The KS-DFT electronic structure calculations for solids are carried out mostly within the semilocal XC approximations, that are usually providing high accuracy with low computational cost. The semilocal approximations are remarkably accurate for many solid-state properties, like equilibrium lattice constants, bulk moduli, cohesive energies, work function, elastic and phonon properties, vacancy formation and surface energies [44–66]. In spite of their accuracy, the semilocal XC functionals actually fail in a few solid-state properties. Within those the lack of accurate prediction of band gap of the semiconductor devices is undoubtedly one of the most important drawbacks of the semilocal approximations. Looking at the rapid development in the semiconductor devices from the technology point of view, the efficient evaluation of the band gap is necessary and still now it is an active research filed with promisingly new prospects.

The poor accuracy of the band gap within the semilocal XC approximations can be inferred from their underestimation of the derivative discontinuity [67–73] and modest description of the delocalization error [74,75]. In KS formalism, the band gap is defined by the difference between the highest occupied molecular orbital (HOMO) and lowest unoccupied molecular orbital (LUMO), i.e., $\Delta_{\rm KS} = \epsilon_{\rm LUMO} - \epsilon_{\rm HOMO}$. For periodic system it becomes $E_g = \epsilon_{\rm CB} - \epsilon_{\rm VB}$, where $\epsilon_{\rm CB}$ and $\epsilon_{\rm VB}$ are the lowest unoccupied and the highest occupied one-electron energies of the conduction and valence bands, respectively. However, the fundamental band gap (E_g) is the difference between ionization potential (IP) and electron affinity (EA). Note that using the variational formalism of DFT, one can obtain the relation between the fundamental band gap and KS gap as $E_g = \Delta_{\rm KS} + \Delta_{\rm xc}$, where $\Delta_{\rm xc}$ is known as the XC derivative discontinuity [76–78]. It was shown in several works [70,71,73,79–82] that inclusion of $\Delta_{\rm xc}$ improves the band gap of solids computed within the LDA or GGA approximations. However, very recently it was proved that meta-GGA implemented in the generalized Kohn-Sham scheme (gKS) includes some amount of the $\Delta_{\rm xc}$ [68,83]. Therefore, meta-GGA functionals may give an improvement in the band gap of solids. It was shown in Ref. [83] that the strongly constrained and appropriately normed (SCAN) [39] and meta-GGA made (very) simple (MVS) [37] improve the band gap, and for several cases the accuracy of MVS is comparable with the expensive hybrid functionals [83]. Note that the meta-GGA XC functionals, being semilocal with respect to KS orbitals, are almost as expensive as the GGA functionals. However, meta-GGA functionals hold additional features, like $\Delta_{\rm xc}$, which make them as preferable candidates to access the band gap problem.

Inspired by the appealing features of these recent meta-GGAs, in this paper, we propose Laplacian-free meta-GGA

*bikash.patra@niser.ac.in
†subrata.jana@niser.ac.in; subrata.niser@gmail.com
‡lucian.constantin@iit.it
§psamal@niser.ac.in

XC functionals using the Becke-Roussel (BR) [28] exchange hole approach. Implementation of these functionals in the gKS shows impressive performance for the semiconductor and insulator band gap. Also, we obtain quite a comparable band gap as obtained from Tran-Blaha modification of the Becke-Johnson exchange potential (TBMBJ) [84] and Heyd-Scuseria-Ernzerhof screened hybrid functional (HSE06) [85–87]. Note that the TBMBJ exchange potential does not have a corresponding exchange functional, whereas hybrid functionals based on the screened nonlocal Hartree-Fock (HF) exchange are quite expensive [85–90]. In this line of development, we also want to acknowledge several other works which improve the band gap performance. Those include Armiento-Kümmel (AK13) functional [19], high local exchange of Verma *et al.* (HLE16) [18], local Slater potential (Sloc) [91], Gritsenko-Leeuwen-Lenthe-Baerends (GLLB) potential [92–94], and DFT $-\frac{1}{2}$ of L. G. Ferreira *et al.* [95]. However, none of these functionals are meta-GGAs and they do not include the Δ_{xc} from the gKS formalism.

In this work, meta-GGA exchange functionals are designed using the BR approach, by suitably modeling the exchange hole and compared it with the hydrogen hole density (H hole density) and cuspless hydrogen hole density (C hole density), respectively. We recall that the hydrogen density is localized because of the cusp [96], whereas the cuspless hydrogen density shows delocalization, being more suitable for the solid-state systems [96]. These functionals are extensively tested for the band gap energies of various solids, from narrow band gap semiconductors to wide-gap insulators, showing systematic improvements over SCAN and MVS meta-GGAs. To present our work, we organize the paper as follows; in Sec. II, we develop the BR-like meta-GGA XC functionals, and in Sec. III, we present and analyze the band-gap results. Finally, in Sec. IV, we summarize our conclusions.

II. LAPLACIAN-FREE BR-LIKE META-GGA FUNCTIONALS

A. Theoretical overview

The exchange energy can be regarded as the electrostatic interaction between the electron spin-σ density $\rho_\sigma(\mathbf{r})$ at reference position $\mathbf{r}$ with spherically averaged exchange hole density $\langle\rho_{x\sigma}(\mathbf{r},\mathbf{r}+\mathbf{u})\rangle$ at $\mathbf{r}+\mathbf{u}$, where $\mathbf{u}$ is the separation between two electrons. So,

$$E_x = -\frac{1}{2}\sum_\sigma \iint \frac{\rho_\sigma(\mathbf{r})\langle\rho_{x\sigma}(\mathbf{r},\mathbf{r}+\mathbf{u})\rangle}{u}\,d\mathbf{r}d\mathbf{u}, \tag{1}$$

where the spherically averaged exchange hole density can be expressed in terms of the first-order Hartree-Fock reduced density matrix as

$$\langle\rho_{x\sigma}(\mathbf{r},\mathbf{r}+\mathbf{u})\rangle = \frac{\langle|\Gamma_{1\sigma}(\mathbf{r},\mathbf{r}+\mathbf{u})|^2\rangle}{\rho_\sigma(\mathbf{r})}, \tag{2}$$

with

$$\langle|\Gamma_{1\sigma}(\mathbf{r},\mathbf{r}+\mathbf{u})|^2\rangle = \frac{1}{4\pi}\int |\Gamma_{1\sigma}(\mathbf{r},\mathbf{r}+\mathbf{u})|^2\,d\Omega_u. \tag{3}$$

The reduced density matrix is expressed in terms the KS orbitals $\psi_{i\sigma}$ as

$$\Gamma_{1\sigma}(\mathbf{r},\mathbf{r}+\mathbf{u}) = \sum_i^{\text{occ}} \psi_{i\sigma}^*(\mathbf{r})\psi_{i\sigma}(\mathbf{r}+\mathbf{u}). \tag{4}$$

We also define the exchange hole potential as the potential generated by the spherically averaged exchange hole at reference point $\mathbf{r}$ and given by

$$U_{x\sigma}(\mathbf{r}) = -\int \frac{\langle\rho_{x\sigma}(\mathbf{r},\mathbf{r}+\mathbf{u})\rangle}{u}\,d\mathbf{u}. \tag{5}$$

Replacing Eq. (5) into Eq. (1), the exchange energy can be written as

$$E_x = \frac{1}{2}\sum_\sigma \int \rho_\sigma(\mathbf{r})U_{x\sigma}(\mathbf{r})d\mathbf{r}. \tag{6}$$

The small $\mathbf{u}$ expansion of the exchange hole is [97,98]

$$\langle\rho_{x\sigma}(\mathbf{r},\mathbf{r}+\mathbf{u})\rangle = \rho_\sigma(\mathbf{r}) + \frac{u^2}{6}\left[\nabla^2\rho_\sigma(\mathbf{r}) - 4\tau_\sigma + \frac{1}{2}\frac{(\vec{\nabla}\rho_\sigma(\mathbf{r}))^2}{\rho_\sigma(\mathbf{r})}\right]. \tag{7}$$

The in-homogeneity parameter used in the Becke-Roussel method [28] is

$$Q_\sigma = \tfrac{1}{6}[\nabla^2\rho_\sigma(\mathbf{r}) - 2\gamma D_\sigma], \tag{8}$$

with $D_\sigma = 2\tau_\sigma - \frac{1}{4}\frac{(\vec{\nabla}\rho_\sigma(\mathbf{r}))^2}{\rho_\sigma(\mathbf{r})}$, and γ being an adjustable parameter and $\tau_\sigma = \frac{1}{2}\sum_i|\nabla\psi_{i\sigma}|^2$.

B. Laplacian free representation of Q_σ

The presence of Laplacian in the above expression makes the exchange hole diverging, especially near the nucleus. To avoid this situation, it is necessary to replace the Laplacian by using the second-order gradient expansion (GE2) of kinetic energy density as

$$\nabla^2\rho_\sigma(\mathbf{r}) \approx 3\left[2\tau_\sigma - \tau_\sigma^{\text{unif}} - \frac{1}{36}\frac{(\vec{\nabla}\rho_\sigma(\mathbf{r}))^2}{\rho_\sigma(\mathbf{r})}\right], \tag{9}$$

where $\tau_\sigma^{\text{unif}} = \frac{3}{5}k_{F\sigma}{}^2\rho_\sigma$, with $k_{F\sigma} = (6\pi^2\rho_\sigma)^{1/3}$. Note that in order to be consistent with the original BR method [28], we use here $\tau_\sigma([\rho_\sigma],\mathbf{r}) = \tau([\rho = 2\rho_\sigma],\mathbf{r})$. We also recall that there exist various τ-dependent approximations of $\nabla^2\rho_\sigma(\mathbf{r})$ [99–103], for simplicity, we discuss only the GE2 expression of Eq. (9).

Replacing Eq. (9) into Eq. (8), we obtain

$$Q_\sigma = \left(\frac{1}{2} - 2\gamma\right)\tau_\sigma' - \frac{1}{2}\tau_\sigma^{\text{unif}} + \left(\frac{\gamma}{2} - \frac{1}{12}\right)\frac{|\nabla\rho_\sigma|^2}{\rho_\sigma}, \tag{10}$$

where $\tau_\sigma' = 2\tau_\sigma$. Let us consider the following generalization of Eq. (10):

$$Q_\sigma = a_1\tau_\sigma' - \frac{1}{2}\tau_\sigma^{\text{unif}} + a_2\frac{|\nabla\rho_\sigma|^2}{\rho_\sigma} + a_3\frac{|\nabla\rho_\sigma|^4}{\rho_\sigma^{11/3}}, \tag{11}$$

where we also add a fourth-order gradient [104,105] contribution to Q_σ. Equation (11) will be used in our functional

development, and the parameters will be fixed from several conditions, as discussed in the next section.

C. BR-like meta-GGA exchange functionals

1. The case of hydrogen hole density

Using the hydrogen density [96]

$$\rho^H(r) = \frac{\alpha^3}{8\pi} e^{-\alpha r} \tag{12}$$

and the hydrogen exchange hole [28]

$$\rho_x^H(r,u) = \frac{\alpha}{16\pi ru}\{e^{-\alpha|r-u|}(\alpha|r-u|+1) - e^{-\alpha(r+u)}(\alpha(r+u)+1)\}, \tag{13}$$

the BR nonlinear equation is obtained as [28]

$$\frac{x\exp(-2x/3)}{x-2} = \frac{2}{3}\pi^{2/3}\frac{\rho_\sigma^{5/3}}{Q_\sigma}, \tag{14}$$

where Q_σ is given by Eq. (11). This nonlinear equation can be solved numerically by using efficient numerical root finding technique,or analytic representation as given in Ref. [106], for each value of density, gradient of density and kinetic energy density. In fact, for the hydrogen density, we use the analytic representation given in Ref. [106]. Now, solving Eq. (14), one can obtain x and the corresponding b as

$$b^3 = \frac{x^3\exp(-x)}{8\pi\rho_\sigma}. \tag{15}$$

The exchange hole potential is given by

$$U_{x\sigma}^H(\mathbf{r}) = -\left(1 - e^{-x} - \frac{1}{2}xe^{-x}\right)/b, \tag{16}$$

and the meta-GGA exchange functional is given by substituting Eq. (16) into Eq. (6). We note that x is dimensionless ingredient, dependent on ρ_σ, $\nabla\rho_\sigma$, and τ_σ. Consequently, the exchange energy behaves properly under a uniform density scaling [107] (i.e., $E_x[\rho_\lambda] = \lambda E_x[\rho]$, with $\rho_\lambda(\mathbf{r}) = \lambda^3\rho(\lambda\mathbf{r})$, $\lambda \geqslant 0$).

The parameters a_1 and a_2 that enter in the expression of Q_σ, are analytically found from the following exact conditions.

(i) For a constant density [$\rho_\sigma(\mathbf{r}) = \rho_{\sigma,0}$, $\nabla\rho_\sigma = 0$, $\tau_\sigma' = \tau_\sigma^{\rm unif}$], the exchange hole potential should recover the LDA behavior, $U_{x\sigma}^H(\mathbf{r}) = U_{x\sigma}^{\rm LDA}(\mathbf{r}) = -3(\frac{3}{4\pi})^{1/3}\rho_\sigma^{1/3}$.

(ii) For a slowly varying density ($\rho_\sigma(\mathbf{r}) = \rho_{\sigma,0} + \delta\rho_\sigma(\mathbf{r})$, with $\delta\rho_\sigma(\mathbf{r}) \ll \rho_\sigma(\mathbf{r})$ and $s_\sigma = |\nabla\rho_\sigma|/[2k_{F\sigma}\rho_\sigma] \leqslant 1$), the exchange functional should recover the modified second-order gradient expansion (MGE2), which ensures an accurate behavior for large atoms and for the Thomas-Fermi density scaling [22,108–111].

Details of the calculations implying (i) and (ii) are provided in Appendix A. Finally, the remaining parameter a_3 has been fitted to the band gap energies of a small test set of bulk solids, which contains C, Si, Ge, InAs, AgBr, and Ne. We choose these solids for a realistic reason: to match the band gap values closely to that of the narrow (InSb, Si, InAs), intermediate (C, AgBr), and wide band gap solids (Ne). More specifically, we choose the value of a_3 to get well balanced band gaps of all the ranges of materials, starting from narrow to wide band gap solids. The parameters of present functional are reported in Table I. We named the functional as modified Becke-Roussel exchange with hydrogen hole density for the band gap of solids (mBRxH-BG).

TABLE I. Parameters values for the proposed exchange energy functionals.

	a_1	a_2	a_3
mBRxH-BG	0.23432	0.089	0.0053
mBRxC-BG	0.074746	0.147	0.0032

2. The case of cuspless hydrogen hole density

For the cuspless hydrogen (C) density [96,112]

$$\rho^C(r) = \frac{\alpha^3}{32\pi} e^{-\alpha r}(1+\alpha r), \tag{17}$$

the exchange hole is

$$\rho_x^C(r,u) = \frac{\alpha}{64\pi ru}\{e^{-\alpha|r-u|}[\alpha^2(r-u)^2 + 3\alpha|r-u| + 3] - e^{-\alpha(r+u)}[\alpha^2(r+u)^2 + 3\alpha(r+u) + 3]\}. \tag{18}$$

Using the BR approach, we find the following nonlinear equation implying the C hole density,

$$\frac{(1+x)^{\frac{5}{3}}}{(x-3)}e^{-2x/3} = (32\pi)^{2/3}\frac{1}{6}\frac{\rho_\sigma^{5/3}}{Q_\sigma}, \tag{19}$$

and the corresponding exchange hole potential is given by

$$U_{x\sigma}^C = -\frac{1}{8b}e^{-x}(-x^2 - 5x + 8e^x - 8), \tag{20}$$

with

$$b^3 = \frac{x^3(1+x)e^{-x}}{32\pi\rho_\sigma}. \tag{21}$$

The meta-GGA exchange functional, named modified Becke-Roussel exchange with C hole density for the band gap of solids (mBRxC-BG), is found by substituting Eq. (20) into Eq. (6). The parameters a_1, a_2, and a_3, reported in Table I, were found using same conditions as before. For details on computing the nonempirical a_1 and a_2, see Appendix A.

D. Comparison between mBRxH-BG and mBRxC-BG meta-GGA exchange functionals

In the upper panel of Fig. 1, we show a comparison between the H and C densities and their reduced gradients. Due to the nuclear cusp, the H density is more localized and its reduced gradient increases monotonically from the minimum value located at the nucleus ($s^H \geqslant s_{\rm min}^H \approx 0.376$). This feature may be an important limitation of mBRxH-like functionals applied to solid-state systems, because in bulk solids s can be smaller than $s_{\rm min}^H$. This shortcoming is resolved by the C density, that is more delocalized and its reduced gradient does not have a finite threshold, spanning all possible values of s ($s^C \geqslant 0$).

In the lower panel of Fig. 1, we show a comparison of the mBRxH-BG and mBRxC-BG exchange enhancement

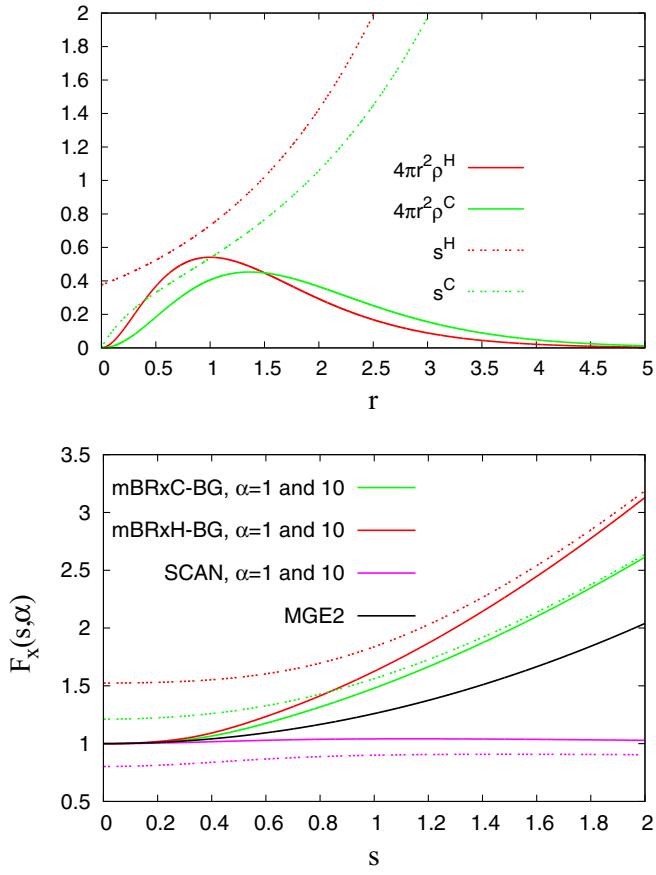

FIG. 1. (Top) The electron probability distributions ($4\pi r^2\rho$) and the reduced gradients ($s_\sigma = |\nabla\rho_\sigma|/[2k_{F\sigma}\rho_\sigma]$) of the hydrogen [see Eq. (12)] and cuspless hydrogen [see Eq. (17)] densities with $\alpha = 2$. (Bottom) Comparison of the mBRxH-BG and mBRxC-BG exchange enhancement factors $F_x(s,\alpha)$. Also shown, are the MGE2 ($F_x^{\rm MGE2} = 1 + 0.26s^2$), and the SCAN meta-GGA exchange enhancement factors. Solid and interrupted lines represent $\alpha = 1$ and 10 cases, respectively.

factors $F_x(s,\alpha) = \epsilon_x/\epsilon_x^{\rm LDA}$, with ϵ_x being the exchange energy per particle, defined as $E_x = \int d\mathbf{r}\ \rho\epsilon_x$. Here, $\alpha = (\tau - \tau^W)/\tau^{\rm unif}$ is the well known meta-GGA ingredient, with $\tau^W = \tau^{\rm unif} 5s^2/3$ being the von Weizsäcker kinetic energy density. Due to the fourth-order gradient expansion term present in Eq. (11), both mBRxH-BG and mBRxC-BG enhancement factors are bigger than MGE2 one, and only when $\alpha \approx 1$ and $s \leqslant 0.5$, they recover MGE2, by construction. Nevertheless, such large enhancement with respect to LDA, which was obtained from the fitting of a_3 parameter to band gap energies of few solids, shows that mBRxH-BG and mBRxC-BG are not suitable for computing most of ground-state properties. In fact, even MGE2 is inaccurate for solid-state calculations, and it needs a negative fourth-order term (i.e., MGE4) present in the SG4 GGA functional [22]. However, more sophisticated expressions for Q_σ of Eq. (11), and inclusion of other exact conditions, may induce a better overall accuracy of meta-GGA functionals, but in this study we focus solely on the band gap energies of bulk solids. Finally, we remark that mBRxC-BG enhancement factor behaves significantly better than mBRxH-BG one, which shows that the C hole density is more suitable for the BR approach applied to solid-state calculations.

III. RESULTS AND DISCUSSIONS

Regarding the correlation, we use one-electron self-interaction free Tao-Perdew-Staroverov-Scuseria (TPSSc) [32] meta-GGA correlation. However, the choice of other correlation functional, as meta-GGA made simple (MSc) [37], or SCAN (SCANc) [39], is also possible. But, we observe that TPSSc correlation is suitably fitted with the mBRxBG exchange functional for the narrow and intermediate band gap solids. To test the performance of the mBRxH-BG and mBRxC-BG meta-GGA XC functionals, we implement them in the plane wave pseudopotential code Vienna *ab initio* simulation package (VASP) [128–131]. We consider $15 \times 15 \times 15$ Monkhorst-Pack k-point mesh, and the 700 eV energy cutoff. Note that the used projector augmented-wave (PAW) potential includes scalar relativistic effects in its pseudopotential. The effects due to the spin-orbit coupling (SOC) have been taken into consideration, using the approach of Ref. [132], where it was shown that subtraction of the SOC corrected values as obtained only from PBE functional is quite reasonable. In particular, the SOC plays an important role in the narrow bandgap semiconductors. Note that SOC tends to lower the calculated band gap [132,133]. The implementation of the proposed functionals are done in the gKS framework according to the scheme provided in Appendix B.

For the benchmark band gap calculations, we consider 15 narrow band gap semiconductors (with 0 eV $\leqslant$ E_g $\leqslant$ 2 eV), 30 intermediate band gap semiconductors (with 2.0 eV $\leqslant$ E_g $\leqslant$ 6.5 eV), 9 ionic wide-band gap solids (with 7.0 eV $\leqslant$ E_g $\leqslant$ 14.2 eV), 4 rare-gas crystals insulators (with 9.2 eV $\leqslant$ E_g $\leqslant$ 21.5 eV), and 9 layered materials (with 1.0 eV $\leqslant$ E_g $\leqslant$ 3.0 eV). All the results are reported in Table II, with the exception of layered materials that are shown in Table III.

To test the convergence of the constructed meta-GGAs we plot in Fig. 2 the band gap of diamond with respect to the plane wave energy cutoff, k mesh, and iteration loop number. For these convergence tests, we employed the mBJLDA as well as the mBRxH-BG and mBRxC-BG in VASP code. While for the rest of the paper the bandgap calculations for mBJLDA are performed in WIEN2k [123] which uses full-potential (linearized) augmented plane-wave ((L)APW) + local orbitals (lo) method. Note that the VASP and WIEN2k results match closely with each other [133]. From Fig. 2, it is clearly evident that all methods show smooth convergence starting from the 400-eV energy cutoff. Overall, mBRxH-BG and mBRxC-BG perform better than mBJLDA, showing smoother convergence with respect to the k mesh. Moreover, we observe that both mBRxH-BG and mBRxC-BG converge well within seven iteration steps, while mBJLDA takes around ten steps to converge.

A. Narrow band gap materials

The narrow band gap solids are very important for technology. From Table II and the upper panel of Fig. 3, we observe that mBRxC-BG provides reasonably well band gap values, being better than mBRxH-BG, SCAN and MVS meta-GGAs,

TABLE II. The band gaps of various semiconductors and insulators as obtained using different levels of approximations. All calculations are performed at the experimental lattice constants given in Refs. [113–121]. The effects due to spin-orbit coupling (SOC) has been taken into consideration by subtracting the SOC correction calculated by PBE functional (given in parentheses). The SOC uncorrected mBJLDA and HSE06 values are taken from Ref. [122] and corrected for SOC as obtained in this work. We also report, for each class of solids, the mean absolute error (MAE) in eV, and the mean absolute relative error [MARE (in percent)]. The experimental band gap values are taken from Ref. [122].

Solids	PBE (SOC)	SCAN (gKS)	MVS (gKS)	mBJLDA [122]	mBRxH-BG (gKS)	mBRxC-BG (gKS)	HSE06 [122]	Expt.
				Narrow band gaps (0–2 eV)				
InSb	−0.23 (0.23)	−0.23	1.38	0.24	0.12	0.16	0.22	0.24
SnTe	−0.11 (0.18)	−0.11	0.21	−0.03	0.26	0.17	−0.01	0.36
InAs	−0.11 (0.11)	−0.06	1.29	0.56	0.47	0.47	0.34	0.42
InN (Wurzite)	0.03 (0.00)	0.12	0.51	0.89	0.13	0.29	0.70	0.72
Ge	0.00 (0.08)	0.16	1.06	0.75	0.27	0.40	0.74	0.74
GaSb	0.00 (0.17)	0.02	1.32	0.78	0.35	0.42	0.71	0.82
SnSe	0.55 (0.03)	0.78	0.95	0.86	1.22	1.17	0.95	0.90
ScN	−0.09 (0.09)	0.17	0.30	0.79	0.16	0.35	0.81	0.90
Si	0.59 (0.00)	0.84	0.93	1.15	1.74	1.59	1.17	1.17
InP	0.71 (0.03)	1.06	1.96	1.59	1.76	1.71	1.40	1.42
BAs	1.10 (0.07)	1.34	1.41	1.64	1.81	1.85	1.79	1.46
GaAs	0.49 (0.11)	0.76	2.08	1.53	1.09	1.14	1.29	1.52
CdTe	0.50 (0.26)	0.76	2.22	1.53	1.66	1.61	1.31	1.61
AlSb	0.99 (0.21)	1.16	1.62	1.54	2.10	1.97	1.59	1.69
CdSe	0.51 (0.12)	0.87	1.93	1.87	2.05	1.90	1.40	1.85
MAE	0.73	0.54	0.40	0.10	0.35	0.27	0.14	
MARE	84.80	69.55	71.64	15.32	38.22	31.39	16.66	
				Intermediate band gaps (>2–6.5 eV)				
BP	1.24 (0.00)	1.54	1.42	1.85	1.82	1.93	1.98	2.10
Cu_2O	0.41 (0.09)	0.43	0.49	0.72	0.56	0.57	1.89	2.17
AlAs	1.34 (0.12)	1.64	2.40	2.01	2.87	2.64	1.99	2.23
GaP	1.60 (0.03)	1.85	2.16	2.22	2.53	2.52	2.25	2.35
ZnTe	1.00 (0.27)	1.32	2.79	2.15	1.83	1.88	1.98	2.39
SiC	1.35 (0.00)	1.71	1.84	2.25	1.89	2.25	2.23	2.42
MgSe	1.76 (0.14)	2.39	3.01	2.79	3.44	3.24	2.60	2.47
CdS	1.16 (0.00)	1.52	2.29	2.67	3.09	2.84	2.14	2.50
AlP	1.56 (0.04)	1.91	2.17	2.27	3.22	3.00	2.26	2.50
AgCl	0.86 (0.04)	1.29	1.85	2.91	2.96	2.69	2.37	3.25
AgBr	0.60 (0.08)	1.08	1.81	2.42	2.35	2.22	1.93	2.71
ZnSe	1.16 (0.12)	1.63	2.72	2.63	2.37	2.35	2.25	2.82
AgI	1.10 (0.23)	1.41	2.43	2.54	2.96	2.76	2.25	2.91
CuBr	0.33 (0.03)	0.63	1.14	1.53	1.82	1.68	2.12	3.07
BaTe	1.26 (0.27)	1.60	1.98	2.01	3.43	2.72	2.04	3.08
CuI	0.98 (0.16)	1.32	2.18	2.04	2.21	2.16	2.49	3.12
GaN	1.72 (0.00)	2.09	2.53	2.85	1.56	2.03	2.85	3.28
CuCl	0.38 (0.07)	0.64	1.00	1.62	2.14	1.90	2.30	3.40
ZnO (Wurzite)	0.77 (0.00)	1.14	1.47	2.65	1.55	1.66	2.50	3.44
GaN (Wurzite)	1.99 (0.00)	2.36	2.82	3.17	1.96	2.36	3.15	3.50
MgTe	2.23 (0.26)	2.84	3.40	3.35	4.84	4.37	3.13	3.60
BaSe	1.75 (0.15)	2.12	2.49	2.71	4.00	3.31	2.64	3.58
ZnS	2.09 (0.00)	2.60	3.34	3.65	3.69	3.57	3.30	3.84
BaS	2.07 (0.05)	2.43	2.75	3.22	4.53	3.87	3.06	3.88
MgS	3.56 (0.00)	4.23	4.68	5.17	7.09	6.23	4.66	4.78
AlN	3.38 (0.00)	3.99	4.17	4.88	3.84	4.41	4.55	4.90
LiH	2.98 (0.00)	3.61	4.08	5.06	6.78	5.86	4.06	4.94
C	4.13 (0.00)	4.54	4.10	4.92	4.66	4.75	5.26	5.50
AlN (Wurzite)	4.15 (0.00)	4.81	5.15	5.51	4.54	5.04	5.49	6.19
BN	4.47 (0.00)	4.96	5.06	5.80	5.29	5.62	5.76	6.36
MAE	1.66	1.25	0.86	0.52	0.91	0.71	0.53	
MARE	50.93	38.71	26.00	16.42	26.77	21.70	16.05	

TABLE II. *(Continued.)*

Solids	PBE (SOC)	SCAN (gKS)	MVS (gKS)	mBJLDA [122]	mBRxH-BG (gKS)	mBRxC-BG (gKS)	HSE06 [122]	Expt.
				Ionic wide-band gap solids				
CaO	3.65 (0.00)	4.22	4.59	5.35	4.72	4.70	5.26	7.00
MgO	4.76 (0.00)	5.60	6.01	7.13	6.08	6.22	6.47	7.83
Kcl	5.15 (0.04)	5.74	6.70	8.44	11.08	10.08	6.49	8.50
NaCl	5.13 (0.04)	5.89	6.79	8.41	11.54	9.62	6.57	8.50
LiCl	6.37 (0.03)	7.26	7.97	8.61	10.92	9.74	7.78	9.40
BeO (Wurzite)	7.51 (0.00)	8.36	8.59	9.66	8.52	8.89	9.48	10.60
KF	6.10 (0.09)	6.68	7.48	10.31	11.72	11.15	8.09	10.90
NaF	6.35 (0.04)	7.09	7.91	11.42	11.99	10.33	8.53	11.50
LiF	9.20 (0.03)	10.09	10.69	12.86	13.22	12.14	11.43	14.20
MAE	3.80	3.05	2.41	0.69	1.73	1.35	2.04	
MARE	39.06	31.25	24.49	7.45	19.50	14.66	20.83	
				Rare gas solids				
Xe	5.80 (0.44)	6.47	7.75	8.04	11.91	10.82	7.00	9.29
Kr	7.02 (0.23)	7.77	9.12	10.57	15.07	13.67	8.48	11.59
Ar	8.62 (0.06)	9.46	10.86	13.78	18.27	16.39	10.31	14.15
Ne	11.50 (0.12)	12.77	14.47	22.21	28.95	22.27	14.15	21.48
MAE	5.89	5.01	3.58	0.84	4.42	1.66	4.14	
MARE	40.63	34.25	23.44	7.07	30.53	13.48	28.19	

but worse than mBJLDA and HSE06 functionals. In general, the mBRxC-BG slightly overestimates the band gap of such semiconductors, with notable exceptions of Ge, InN, GaAs, GaSb, and ScN where predicts smaller band gap energies. We also observe that for few cases (InSb, InAs, GaSb InP, GaAs, and CdTe) the MVS massively overestimates the band gaps. However, both SCAN and MVS meta-GGAs perform remarkably well. This interesting feature of the SCAN and MVS functionals, is particularly missing in the TPSS functional. We recall that though the TPSS is implemented in the gKS, yet it does not show improvement in the band gap for solids. Note that the SOC inclusion is important especially for various materials, such as CdTe, GaSb, and AlSb.

However, a closer look indicates that for narrow band gap semiconductors the mBRxC-BG provides very good band gap values within the meta-GGA XC functionals, except for few cases (for example, Si). In particular, the interesting feature of the present modifications of BR XC functional is that it predicts nonzero band gaps for all the narrow band gap materials.

B. Intermediate band gap semiconductors

Concerning the intermediate band gap semiconductors, we observe reasonably good performance with the mBRxH-BG and mBRxC-BG functionals. Both the functionals give quite a balanced band gaps values over the different range of materials in this category. However, SCAN has the inherent tendency to underestimate the band gap. MVS gives larger gaps than SCAN, but in most cases still clearly underestimate the gaps. However, this is not the case for the mBRx based XC functionals, which perform better than SCAN and MVS

TABLE III. The band gaps (eV) of different layered materials in their bulk construction as obtained using different levels of approximations. All calculations are done at the experimental geometries. Experimental band gaps are taken from various references are also mentioned. The mBJLDA calculations are performed in WIEN2k code [123]. While the HSE06 calculations are performed in VASP. The effects due to spin-orbit coupling (SOC) has been taken into consideration by subtracting the SOC correction calculated by PBE functional (given in parentheses). Last lines report MAE (eV) and MARE(%).

Solids	PBE (SOC)	SCAN (gKS)	MVS (gKS)	mBJLDA	mBRxH-BG (gKS)	mBRxC-BG (gKS)	HSE06	Expt.
HfS_2	0.94 (0.00)	1.29	1.52	1.64	1.65	1.72	1.70	1.96 [124]
$HfSe_2$	0.32 (0.16)	0.68	0.94	0.90	0.87	0.98	0.98	1.13 [124]
MoS_2	0.91 (0.00)	1.01	1.05	1.12	1.20	1.19	1.46	1.29 [122]
$MoSe_2$	0.85 (0.00)	0.96	1.01	1.02	1.21	1.21	1.33	1.10 [125]
WS_2	0.99 (0.05)	1.18	1.13	1.18	1.40	1.40	1.51	1.35 [126]
WSe_2	0.91 (0.08)	1.11	1.05	1.07	1.35	1.31	1.36	1.20 [126]
ZrS_2	0.81 (0.00)	1.12	1.32	1.26	1.50	1.50	1.59	1.68 [124]
$ZrSe_2$	0.20 (0.13)	0.51	0.74	0.57	0.76	0.78	0.87	1.20 [124]
ZrSeS	0.52 (0.06)	0.83	1.05	1.02	1.14	1.15	1.24	1.40 [127]
MAE	0.65	0.40	0.28	0.28	0.21	0.18	0.19	
MARE	47.26	28.99	20.09	20.70	15.77	13.68	15.85	

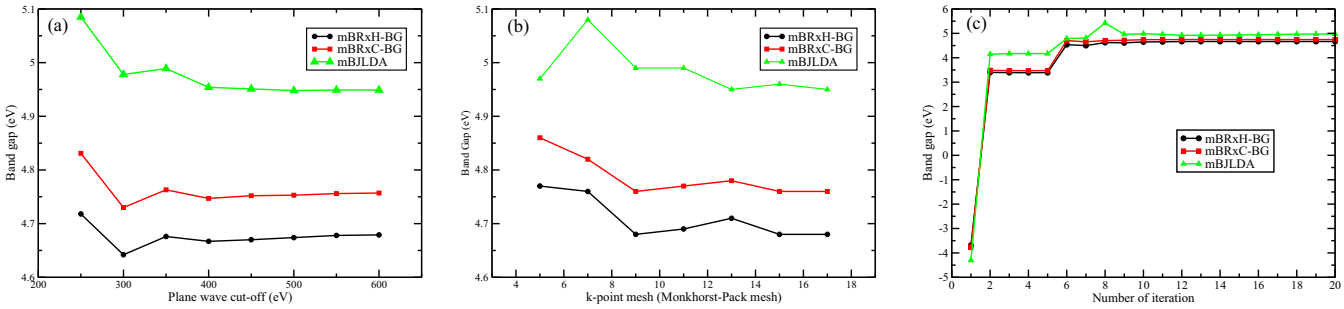

FIG. 2. Comparison of mBRxH-BG, mBRxC-BG and mBJLDA for several tests of convergence, in case of diamond. (a) Plane wave energy cutoff vs band gap convergence; (b) k mesh vs band gap convergence; and (c) iteration steps vs band gap. For (a) and (c), we used the $15 \times 15 \times 15$ Monkhorst-Pack k-point mesh; and for (b) and (c), we used the 700 eV energy cutoff.

for most of the solids, being close to HSE06 and mBJLDA functionals. We observe that the inclusion of the SOC is still important for some materials (e.g., ZnTe, AgI, BaTe, and MgTe), but is below 10% from the experimental value.

To show the overview of the functionals performance, we also plot the results in Fig. 3 (middle panel). Here, we want to mention that the underestimation problem of mBJLDA for the copper compounds (Cu_2O, CuBr, CuI, CuCl) is present in all the semilocal functionals. We also remark the difficult case of GaN, where both mBRxH-BG and mBRxC-BG perform worse than SCAN and MVS.

To encapsulate the physical behavior of the meta-GGA functionals, we compare in Fig. 4(a), the pseudodensity of valence band of diamond along the [111] direction. We also plot in Fig. 4(b) the pseudodensity of conduction-band minima (CBM) and valence-band maxima (VBM) of the diamond (similar with Fig. 5 of Ref. [134]). Note that the pseudodensities do not show the large contribution of the s electrons at the nucleus, as an all-electron density would show. Due to the stronger exchange enhancement, the mBRxC-BG and mBRxH-BG pseudodensities of the valence band [Fig. 4(a)] are slightly lowered with respect to the other curves, in the bonding region, in the range between 3 and 5 Å. However, all curves agree well each other. On the other hand, the CBM pseudodensity of mBRxC-BG deviates significantly from the LDA and SCAN ones, in the same bonding region [see Fig. 4(b)].

C. Ionic wide band gap solids and rare gas crystal insulators

The results are reported in Table II and the lower panel of Fig. 3. Regarding the ionic wide band gap solids, and insulators the mBRxC-BG shows very promising results within the semilocal XC functionals, outperforming not only the SCAN, MVS, and mBRxH-BG meta-GGAs, but also the HSE06 screened hybrid. For insulators, the mBRxC-BG performance is quite close to mBJLDA, being remarkably accurate.

For the comparison purpose, the SCAN and mBRxC-BG band structures of the Ar solid are shown in Fig. 5. The mBRxC-BG not only predicts accurately the band gap of the Ar crystal, but also shows a smooth and physical band structure. We recall that the improvement in the band gap of insulators is mainly due to the fourth order gradient term included in the Q_σ of Eq. (11), which plays important role whenever $s \geqslant 0.5$ (see the lower panel of Fig. 1).

D. Layered materials

Layered materials are important in science and technology, being used in different electronics and optoelectronics devices. Recently, more than 5000 layered materials have been identified [135], and a simple theoretical tool for computing their band gap energies is of interest. We recall that there are several van der Waals corrected GGAs and meta-GGAs accurate for lattice constants and layer-layer binding energies, such as cx13-vdW-DF [136,137], PBEsol + rVV10s [138], and SCAN + rVV10 [139].

In Table III, we report our results. The experimental band gaps are taken from Refs. [122,124–127], being mostly extracted from different experiments, and agreeing well with the fundamental band gaps from GW method [124]. The best functional is mBRxC-BG with MAE = 0.18 eV, followed by HSE06 (MAE = 0.19 eV) and MVS or mBJLDA meta-GGA (both have MAE = 0.28 eV), while mBJLDA performs rather modestly, with MAE = 0.28 eV, showing a systematic underestimation of the band gap energies. It is noteworthy to mention that the underestimation of the band gap of the layered materials is the inherent problem of the mBJLDA. This is due to the averages over the unit cell used in the mBJLDA potential. Very recently, a reparametrized form of the mBJLDA is presented for the layered materials [140]. But SCAN, MVS, mBRxC-BG and hybrid functional are free from such an anomaly. This is quite a remarkable and attractive feature of the mBRxC-BG functional and can be further used for the benchmarking calculations of different layered bulk solids such as layered hybrid organic-inorganic perovskites and topological insulators.

E. Overall statistics

In Table IV, we present the overall error statistics of the band gap energies, evaluated using different functionals, for 67 test cases. We report the mean (relative) error (M(R)E), mean absolute (relative) error (MA(R)E), and the standard deviation of (relative) errors (STD(R)E). We use the standard notation of calculationg those quantities. Regarding the overall statistics, the SCAN meta-GGA have the worst MAE (1.45 eV) and MARE (43.04%) results. Followed by the MVS functional (with MAE = 1.05 eV and MARE = 35.07 eV). However, SCAN gives errors closer to the MARE (with STDRE $\sim$ 31%), while MVS is more unpredictable (STDRE $\sim$ 70%). On the other hand, the mBRxC-BG

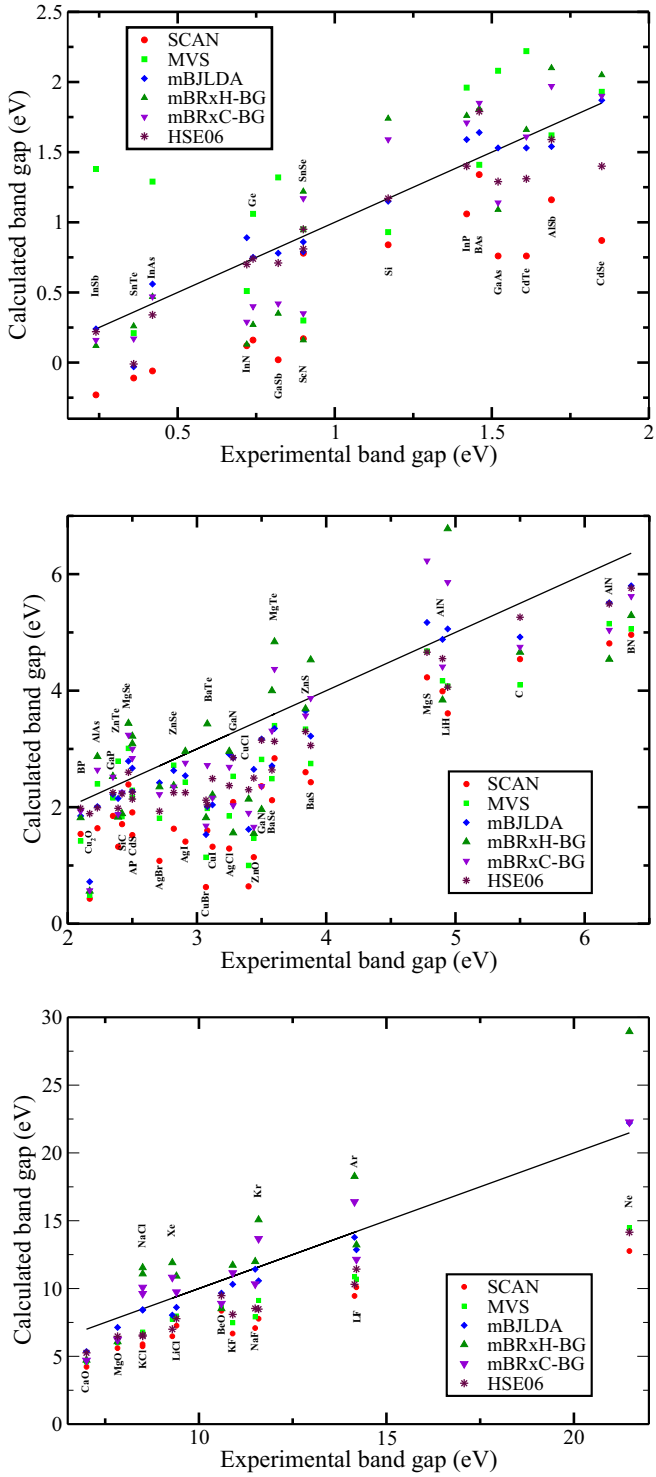

FIG. 3. Experimental vs calculated band gaps for the narrow band gap (top), intermediate band gap (middle), and wide band gap (bottom) materials, using different methods. PBE values are not considered.

meta-GGA is comparable with HSE06 hybrid functional, and slighly worse than mBJLDA meta-GGA potential. We also observe the systematic improvement of mBRxC-BG with respect to mBRxH-BG.

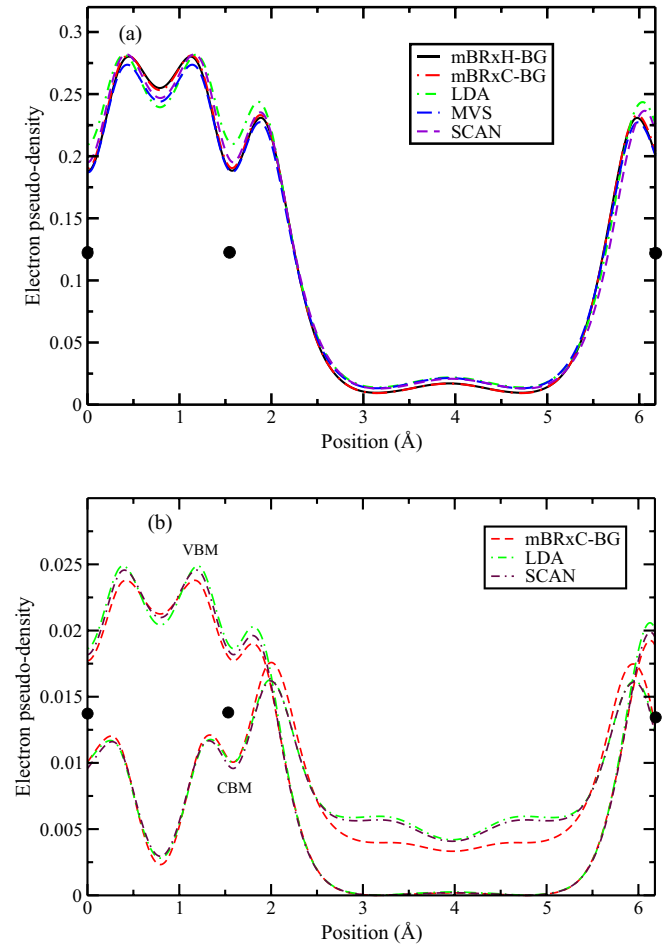

FIG. 4. The electron pseudodensities of the (a) valence-band and (b) conduction-band minima (CBM) and valence-band maxima (VBM) are shown along [111] direction in diamond bulk, as obtained with several XC functionals.

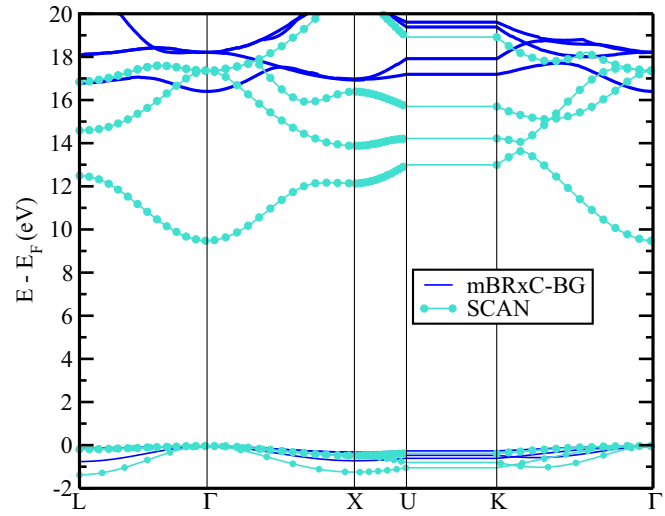

FIG. 5. Band structure of Ar solid using the mBRxC-BG and SCAN exchange-correlation functionals.

TABLE IV. Summary of band gap error statistics of 67 test solids as obtained using different functionals. PBE results are not considered here.

	SCAN (gKS)	MVS (gKS)	mBJLDA	mBRxH-BG (gKS)	mBRxC-BG (gKS)	HSE06
ME (eV)	−1.45	−0.88	−0.37	0.14	−0.17	−0.78
MAE (eV)	1.45	1.05	0.44	1.01	0.69	0.82
STDE (eV)	1.42	1.29	0.50	1.55	0.91	1.19
MRE (%)	−43.04	−6.55	−11.46	−5.73	−8.80	−14.59
MARE (%)	43.04	35.07	14.99	27.11	21.35	17.39
STDRE (%)	31.23	69.81	20.14	32.18	25.16	16.66

IV. CONCLUSIONS

To summarize, a generalized Kohn-Sham overview of the band gap of solids is proposed using the modified Becke-Roussel meta-GGA exchange functionals, named mBRxH-BG and mBRxC-BG, coupled with the hydrogen and cuspless hydrogen hole densities, respectively. The second-order coefficient of the **u** expansion of the exchange hole, denoted Q_σ, has been made Laplacian free, and generalized [see Eq. (11)] in order to ensure that the mBRxH-BG and mBRxC-BG meta-GGA functionals will satisfy several exact conditions. This method of developing exchange functionals should be further investigated considering more sophisticated expressions for Q_σ, that will allow the recovery of other exact conditions.

The mBRxH-BG and mBRxC-BG meta-GGA exchange functionals, combined with the TPSS correlation, have been assessed for the band gap energies of a large palette of bulk solids, from narrow to wide band gap solids, and from strongly packed to noncovalently bound layered materials, and van der Waals rare gas crystals. The overall performance of mBRxC-BG is significantly superior to the mBRxH-BG, SCAN and MVS meta-GGAs ones, and close to the ones of the best known approaches (the mBJLDA potential and the HSE06 screened hybrid functional). These results showed that the mBRxC-BG functional could be a potential substitution of hybrid functional for calculating the band gaps of semiconductors with computationally less time.

APPENDIX A: THE NONEMPIRICAL PARAMETERS a_1 AND a_2 OF mBRxH-BG AND mBRxC-BG FUNCTIONALS

1. mBRxH-BG meta-GGA

For uniform electron gas $Q_{\sigma 0} = (a_1 - \frac{1}{2})\tau_\sigma^{\rm unif}$. Putting this value in Eq. (14), we get

$$a_1 - \frac{1}{2} = K_0 \frac{x_0 - 2}{x_0 e^{-2x_0/3}}, \tag{A1}$$

where $K_0 = \frac{10(\pi)^{2/3}}{9(6\pi^2)^{2/3}} = 0.156876$.

From the condition $U_{x\sigma}^H(\mathbf{r}) = U_{x\sigma}^{\rm LDA}(\mathbf{r}) = -3(\frac{3}{4\pi})^{1/3}\rho_\sigma^{1/3}$, we obtain

$$\frac{e^{x_0/3}}{x_0}\left(1 - e^{-x_0} - \frac{1}{2}x_0 e^{-x_0}\right) = K_1, \tag{A2}$$

where $K_1 = 3(\frac{3}{4\pi})^{1/3}\frac{1}{(8\pi)^{1/3}} = 0.635348$. We find the solution of above non linear equation resulting $x_0 = 1.104301$. Putting the value of x_0 in Eq. (A1), we obtain

$$a_1 = \tfrac{1}{2} - 0.26568 = 0.23432. \tag{A3}$$

Now, let consider a small, long wave length, perturbation of the uniform electron gas. Then, $Q_\sigma = Q_{\sigma 0} + Q_{\sigma 1}$, and $x = x_0 + x_1$, with $Q_{\sigma 1} \ll Q_{\sigma 0}$, and $x_1 \ll x_0$. Note that $x_0 = 1.104301$, and $Q_{\sigma 0} = (a_1 - \frac{1}{2})\tau_\sigma^{\rm unif}$. Considering the gradient expansion of Eq. (11), we find

$$Q_{\sigma 1} = \left(\frac{a_1}{36} + a_2\right)\frac{|\nabla\rho_\sigma|^2}{\rho_\sigma}. \tag{A4}$$

Taking the Taylor expansion of Eq. (14), and considering only the linear terms, we obtain

$$e^{-2x_0/3}\frac{(x_0^2 - 2x_0 + 3)}{(x_0 - 2)^2}x_1 = \pi^{2/3}\frac{\rho_\sigma^{5/3}}{{Q_{\sigma 0}}^2}Q_{\sigma 1}, \tag{A5}$$

which defines $x_1 = 0.305(\frac{a_1}{36} + a_2)\frac{|\nabla\rho_\sigma|^2}{\rho_\sigma^{8/3}}$. Taking the Taylor expansion of $U_{x\sigma}^H$ [see Eq. (16)], we finally obtain

$$\begin{aligned} U_{x\sigma}^H &= {U_{x\sigma 0}}^H + {U_{x\sigma 1}}^H = -1.861\rho_\sigma^{1/3} - 0.272\rho_\sigma^{1/3}x_1 \\ &= -1.861\rho_\sigma^{1/3} - 0.0830\left(\frac{a_1}{36} + a_2\right)\rho_\sigma^{1/3}\frac{|\nabla\rho_\sigma|^2}{\rho_\sigma^{8/3}}. \end{aligned} \tag{A6}$$

On the other hand, the second-order gradient expansion [22,141] is $\epsilon_{x\sigma} = -1.861\rho_\sigma^{1/3} - 0.0306\mu_x\rho_\sigma^{1/3}\frac{|\nabla\rho_\sigma|^2}{\rho_\sigma^{8/3}}$, where μ_x is the second-order coefficient ($\mu_x = 10/81$ for GE2 [142], and $\mu_x = 0.26$ for MGE2 [22,108]). Then the mBRxH-BG functional recovers MGE2 if

$$a_2 = -\frac{a_1}{36} + \frac{0.0306}{0.0830}\mu_x \approx 0.089. \tag{A7}$$

2. mBRxC-BG meta-GGA

Using $Q_{\sigma 0}$ in Eq. (19), we obtain

$$a_1 - \frac{1}{2} = K_0\frac{x_0 - 3}{(1 + x_0)^{1/3}e^{(-2x_0/3)}}, \tag{A8}$$

where $K_0 = \frac{5(32\pi)^{2/3}}{18(6\pi^2)^{2/3}} = 0.39530296$.

From the condition $U_{x\sigma}^C(\mathbf{r}) = U_{x\sigma}^{\rm LDA}(\mathbf{r}) = -3(\frac{3}{4\pi})^{1/3}\rho_\sigma^{1/3}$, we obtain

$$\frac{e^{-2x_0/3}}{x_0(1 + x_0)^{1/3}}\left(-x_0^2 - 5x_0 + 8e^{x_0} - 8\right) = K_1, \tag{A9}$$

where $K_1 = 24(\frac{3}{4\pi})^{1/3}\frac{1}{(32\pi)^{1/3}} = 3.2019539$.

Using Newton-Raphson method we find the solution of above non linear equation resulting $x_0 = 1.201014$. Putting the value of x_0 in Eq. (A8), we find

$$a_1 = \tfrac{1}{2} - 0.425254 = 0.074746. \tag{A10}$$

Performing the same linearization procedure as in H case, we obtain

$$4e^{-2x_0/3}\frac{(x_0^2-3x_0+6)(1+x_0)^{2/3}}{(x_0-3)^2}x_1=(32\pi)^{2/3}\frac{\rho_\sigma^{5/3}}{{Q_{\sigma 0}}^2}Q_{\sigma 1}, \tag{A11}$$

such that $x_1=0.4(\frac{a_1}{36}+a_2)\frac{|\nabla\rho_\sigma|^2}{\rho_\sigma^{8/3}}$, and

$$U_{x\sigma}^C=-1.861\rho_\sigma^{1/3}-0.0532\left(\frac{a_1}{36}+a_2\right)\rho_\sigma^{1/3}\frac{|\nabla\rho_\sigma|^2}{\rho_\sigma^{8/3}}. \tag{A12}$$

Finally, we obtain

$$a_2=-\frac{a_1}{36}+\frac{0.0306}{0.0532}\mu_x\approx 0.147. \tag{A13}$$

APPENDIX B: FUNCTIONAL DERIVATIVES OF THE PRESENT BECKE-ROUUSEL MODEL

In Ref. [57], the self-consistent implementation of the meta-GGA functionals are presented. Here we only give the analytic presentation of the derivatives of the BR type functional. Unlike the BR potential, the modified version of it contains only the density, gradient of density and Kohn-Sham kinetic energy density. So, like other meta-GGA type semilocal functionals one can implement it using generalized KS (gKS) scheme. The scheme of calculating the functional derivatives of BR exchange functional is discussed by Neumann *et al.* [143]. Here, we only discuss about the derivatives which are involved in our calculation. In gKS prescription, the potential is given by

$$\begin{aligned}v_x\Psi_i^{\rm KS}=&\frac{\partial\left(\frac{1}{2}\rho_\sigma U_{X\sigma}\right)}{\partial\rho_\sigma}\Psi_i^{\rm KS}\\&-\vec{\nabla}\cdot\left[\frac{\partial\left(\frac{1}{2}\rho_\sigma U_{X\sigma}\right)}{\partial\vec{\nabla}\rho_\sigma}\Psi_{i\sigma}^{\rm KS}+\frac{\partial\left(\frac{1}{2}\rho_\sigma U_{X\sigma}\right)}{\partial\tau_\sigma^{\rm KS}}\vec{\nabla}\Psi_{i\sigma}^{\rm KS}\right]\\&+\left(\frac{\partial\left(\frac{1}{2}\rho_\sigma U_{X\sigma}\right)}{\partial\vec{\nabla}\rho_\sigma}\right)\cdot\vec{\nabla}\Psi_{i\sigma}^{\rm KS}\end{aligned} \tag{B1}$$

and the exchange energy is given by

$$\begin{aligned}E_x&=\frac{1}{2}\sum_{i=1}^{\sigma}\int\rho_\sigma(\mathbf{r})U_{X\sigma}\,d^3r,\\&=\sum_{i=1}^{\sigma}\int G[\rho_\sigma,x]\,d^3r,\end{aligned} \tag{B2}$$

where, for the mBRxH-BG meta-GGA functional,

$$G[\rho_\sigma,x]=-\frac{1}{2}\rho_\sigma\left(1-e^{-x}-\frac{1}{2}xe^{-x}\right)\Big/b \tag{B3}$$

with $b=[\frac{x^3\exp(-x)}{8\pi\rho_\sigma}]^{1/3}$. So, one needs to calculate $\frac{\partial G}{\partial\rho_\sigma}$, $\frac{\partial G}{\partial|\nabla\rho_\sigma|}$, and $\frac{\partial G}{\partial\tau_\sigma^{\rm KS}}$ separately. Now, using the chain rule of functional derivative, one can write

$$\begin{aligned}\frac{\partial G}{\partial\rho_\sigma}&=\frac{\partial G}{\partial\rho_\sigma}+\frac{\partial G}{\partial x}\frac{\partial x}{\partial\rho_\sigma},\\\frac{\partial G}{\partial|\nabla\rho_\sigma|}&=\frac{\partial G}{\partial|\nabla\rho_\sigma|}+\frac{\partial G}{\partial x}\frac{\partial x}{\partial|\nabla\rho_\sigma|},\\\frac{\partial G}{\partial\tau_\sigma}&=\frac{\partial G}{\partial\tau_\sigma}+\frac{\partial G}{\partial x}\frac{\partial x}{\partial\tau_\sigma}.\end{aligned} \tag{B4}$$

To determine $\frac{\partial x}{\partial\rho_\sigma}$, $\frac{\partial x}{\partial|\nabla\rho_\sigma|}$, and $\frac{\partial x}{\partial\tau_\sigma}$ we have to consider the nonlinear equation of x that is behind the mBRxH-BG functional [see Eq. (14)], which in general way can be written as

$$f(x)=h[\rho_\sigma,|\nabla\rho_\sigma|,\tau_\sigma^{\rm KS}]. \tag{B5}$$

Now,

$$\frac{df(x)}{dx}=\frac{\partial h}{\partial\rho}\frac{\partial\rho}{\partial x}, \tag{B6}$$

which implies that

$$\frac{\partial x}{\partial\rho}=\frac{\partial h}{\partial\rho}\Big/\frac{df(x)}{dx}. \tag{B7}$$

Similarly,

$$\frac{\partial x}{\partial|\nabla\rho_\sigma|}=\frac{\partial h}{\partial|\nabla\rho_\sigma|}\Big/\frac{df(x)}{dx} \tag{B8}$$

and

$$\frac{\partial x}{\partial\tau}=\frac{\partial h}{\partial\tau}\Big/\frac{df(x)}{dx}. \tag{B9}$$

This approach can be applied to any BR-like functional to calculate its derivative.

[1] P. Hohenberg and W. Kohn, Phys. Rev. **136**, B864 (1964).
[2] W. Kohn and L. J. Sham, Phys. Rev. **140**, A1133 (1965).
[3] J. P. Perdew and A. Zunger, Phys. Rev. B **23**, 5048 (1981).
[4] A. D. Becke, Phys. Rev. A **38**, 3098 (1988).
[5] C. Lee, W. Yang, and R. G. Parr, Phys. Rev. B **37**, 785 (1988).
[6] J. P. Perdew, J. A. Chevary, S. H. Vosko, K. A. Jackson, M. R. Pederson, D. J. Singh, and C. Fiolhais, Phys. Rev. B **46**, 6671 (1992).
[7] J. P. Perdew, K. Burke, and M. Ernzerhof, Phys. Rev. Lett. **77**, 3865 (1996).
[8] R. Armiento and A. E. Mattsson, Phys. Rev. B **72**, 085108 (2005).
[9] A. E. Mattsson and R. Armiento, Int. J. Quantum Chem. **110**, 2274 (2010).
[10] L. Vitos, B. Johansson, J. Kollár, and H. L. Skriver, Phys. Rev. B **62**, 10046 (2000).
[11] Z. Wu and R. E. Cohen, Phys. Rev. B **73**, 235116 (2006).
[12] Y. Zhao and D. G. Truhlar, J. Chem. Phys. **128**, 184109 (2008).
[13] L. A. Constantin, A. Terentjevs, F. Della Sala, and E. Fabiano, Phys. Rev. B **91**, 041120(R) (2015).

[14] L. A. Constantin, J. P. Perdew, and J. M. Pitarke, Phys. Rev. B **79**, 075126 (2009).
[15] F. G. Eich, S. Pittalis, and G. Vignale, Phys. Rev. B **88**, 245102 (2013).
[16] B. Hammer, L. B. Hansen, and J. K. Nørskov, Phys. Rev. B **59**, 7413 (1999).
[17] Y. Zhang and W. Yang, Phys. Rev. Lett. **80**, 890 (1998).
[18] P. Verma and D. G. Truhlar, J. Phys. Chem. Lett. **8**, 380 (2017).
[19] R. Armiento and S. Kümmel, Phys. Rev. Lett. **111**, 036402 (2013).
[20] E. Fabiano, P. E. Trevisanutto, A. Terentjevs, and L. A. Constantin, J. Chem. Theory Comput **10**, 2016 (2014).
[21] L. A. Constantin, L. Chiodo, E. Fabiano, I. Bodrenko, and F. D. Sala, Phys. Rev. B **84**, 045126 (2011).
[22] L. A. Constantin, A. Terentjevs, F. Della Sala, P. Cortona, and E. Fabiano, Phys. Rev. B **93**, 045126 (2016).
[23] A. Cancio, G. P. Chen, B. T. Krull, and K. Burke, J. Chem. Phys. **149**, 084116 (2018).
[24] L. Chiodo, L. A. Constantin, E. Fabiano, and F. Della Sala, Phys. Rev. Lett. **108**, 126402 (2012).
[25] L. A. Constantin, J. P. Perdew, and J. M. Pitarke, Phys. Rev. Lett. **101**, 016406 (2008).
[26] L. A. Constantin, Phys. Rev. B **78**, 155106 (2008).
[27] J. Carmona-Espíndola, J. L. Gázquez, A. Vela, and S. B. Trickey, J. Chem. Theory Comput. **15**, 303 (2018).
[28] A. D. Becke and M. R. Roussel, Phys. Rev. A **39**, 3761 (1989).
[29] T. Van Voorhis and G. E. Scuseria, J. Chem. Phys. **109**, 400 (1998).
[30] Y. Zhao and D. G. Truhlar, J. Chem. Phys. **125**, 194101 (2006).
[31] J. P. Perdew, S. Kurth, A. Zupan, and P. Blaha, Phys. Rev. Lett. **82**, 2544 (1999).
[32] J. Tao, J. P. Perdew, V. N. Staroverov, and G. E. Scuseria, Phys. Rev. Lett. **91**, 146401 (2003).
[33] J. P. Perdew, A. Ruzsinszky, G. I. Csonka, L. A. Constantin, and J. Sun, Phys. Rev. Lett. **103**, 026403 (2009).
[34] L. A. Constantin, E. Fabiano, and F. D. Sala, Phys. Rev. B **86**, 035130 (2012).
[35] L. A. Constantin, E. Fabiano, and F. Della Sala, Phys. Rev. B **88**, 125112 (2013).
[36] J. Sun, R. Haunschild, B. Xiao, I. W. Bulik, G. E. Scuseria, and J. P. Perdew, J. Chem. Phys. **138**, 044113 (2013).
[37] J. Sun, J. P. Perdew, and A. Ruzsinszky, Proc. Natl. Acad. Sci. U. S. A. **112**, 685 (2015).
[38] A. Ruzsinszky, J. Sun, B. Xiao, and G. I. Csonka, J. Chem. Theory Comput. **8**, 2078 (2012).
[39] J. Sun, A. Ruzsinszky, and J. P. Perdew, Phys. Rev. Lett. **115**, 036402 (2015).
[40] J. Tao and Y. Mo, Phys. Rev. Lett. **117**, 073001 (2016).
[41] Y. Wang, X. Jin, H. S. Yu, D. G. Truhlar, and X. He, Proc. Natl. Acad. Sci. U. S. A. **114**, 8487 (2017).
[42] P. D. Mezei, G. I. Csonka, and M. Kállay, J. Chem. Theory Comput. **14**, 2469 (2018).
[43] F. Della Sala, E. Fabiano, and L. A. Constantin, Int. J. Quantum Chem. **116**, 1641 (2016).
[44] C. J. Cramer and D. G. Truhlar, Phys. Chem. Chem. Phys. **11**, 10757 (2009).
[45] R. Peverati and D. G. Truhlar, Phil. Trans. R. Soc. A **372**, 20120476 (2014).
[46] V. N. Staroverov, G. E. Scuseria, J. Tao, and J. P. Perdew, J. Chem. Phys. **119**, 12129 (2003).
[47] Y. Zhao, N. E. Schultz, and D. G. Truhlar, J. Chem. Theory Comput. **2**, 364 (2006).
[48] L. Goerigk and S. Grimme, J. Chem. Theory Comput. **7**, 291 (2011).
[49] P. Hao, J. Sun, B. Xiao, A. Ruzsinszky, G. I. Csonka, J. Tao, S. Glindmeyer, and J. P. Perdew, J. Chem. Theory Comput. **9**, 355 (2013).
[50] L. Goerigk, A. Hansen, C. Bauer, S. Ehrlich, A. Najibi, and S. Grimme, Phys. Chem. Chem. Phys. **19**, 32184 (2017).
[51] Y. Mo, G. Tian, R. Car, V. N. Staroverov, G. E. Scuseria, and J. Tao, J. Chem. Phys. **145**, 234306 (2016).
[52] Y. Mo, G. Tian, and J. Tao, Phys. Chem. Chem. Phys. **19**, 21707 (2017).
[53] P. Haas, F. Tran, and P. Blaha, Phys. Rev. B **79**, 085104 (2009).
[54] F. Tran, J. Stelzl, and P. Blaha, J. Chem. Phys. **144**, 204120 (2016).
[55] Y. Mo, R. Car, V. N. Staroverov, G. E. Scuseria, and J. Tao, Phys. Rev. B **95**, 035118 (2017).
[56] A. E. Mattsson, R. Armiento, J. Paier, G. Kresse, J. M. Wills, and T. R. Mattsson, J. Chem. Phys. **128**, 084714 (2008).
[57] J. Sun, M. Marsman, G. I. Csonka, A. Ruzsinszky, P. Hao, Y.-S. Kim, G. Kresse, and J. P. Perdew, Phys. Rev. B **84**, 035117 (2011).
[58] G. I. Csonka, J. P. Perdew, A. Ruzsinszky, P. H. T. Philipsen, S. Lebègue, J. Paier, O. A. Vydrov, and J. G. Ángyán, Phys. Rev. B **79**, 155107 (2009).
[59] S. Jana, A. Patra, and P. Samal, J. Chem. Phys. **149**, 044120 (2018).
[60] S. Jana, K. Sharma, and P. Samal, J. Chem. Phys. **149**, 164703 (2018).
[61] A. Patra, J. E. Bates, J. Sun, and J. P. Perdew, Proc. Natl. Acad. Sci. U. S. A. **114**, E9188 (2017).
[62] J. Sun, B. Xiao, Y. Fang, R. Haunschild, P. Hao, A. Ruzsinszky, G. I. Csonka, G. E. Scuseria, and J. P. Perdew, Phys. Rev. Lett. **111**, 106401 (2013).
[63] S. K. Kwon, Z. Nabi, K. Kádas, L. Vitos, J. Kollár, B. Johansson, and R. Ahuja, Phys. Rev. B **72**, 235423 (2005).
[64] M. Ropo, K. Kokko, and L. Vitos, Phys. Rev. B **77**, 195445 (2008).
[65] J. Kollár, L. Vitos, and H. L. Skriver, Phys. Rev. B **49**, 11288 (1994).
[66] A. Landa, P. Soederlind, I. Naumov, J. Klepeis, and L. Vitos, Computation **6**, 29 (2018).
[67] J. P. Perdew, R. G. Parr, M. Levy, and J. L. Balduz, Phys. Rev. Lett. **49**, 1691 (1982).
[68] J. P. Perdew, W. Yang, K. Burke, Z. Yang, E. K. U. Gross, M. Scheffler, G. E. Scuseria, T. M. Henderson, I. Y. Zhang, A. Ruzsinszky, H. Peng, J. Sun, E. Trushin, and A. Görling, Proc. Natl. Acad. Sci. U.S.A. **114**, 2801 (2017).
[69] L. J. Sham and M. Schlüter, Phys. Rev. Lett. **51**, 1888 (1983).
[70] J. P. Perdew and M. Levy, Phys. Rev. Lett. **51**, 1884 (1983).
[71] D. J. Tozer, J. Chem. Phys. **119**, 12697 (2003).
[72] M. E. Casida, C. Jamorski, K. C. Casida, and D. R. Salahub, J. Chem. Phys. **108**, 4439 (1998).
[73] E. Kraisler and L. Kronik, J. Chem. Phys. **140**, 18A540 (2014).
[74] P. Mori-Sánchez, A. J. Cohen, and W. Yang, Phys. Rev. Lett. **100**, 146401 (2008).
[75] M. K. Y. Chan and G. Ceder, Phys. Rev. Lett. **105**, 196403 (2010).

[76] A. Seidl, A. Görling, P. Vogl, J. A. Majewski, and M. Levy, Phys. Rev. B **53**, 3764 (1996).
[77] A. Görling and M. Levy, Phys. Rev. A **52**, 4493 (1995).
[78] M. Levy and F. Zahariev, Phys. Rev. Lett. **113**, 113002 (2014).
[79] G. K.-L. Chan, J. Chem. Phys. **110**, 4710 (1999).
[80] M. J. Allen and D. J. Tozer, Mol. Phys. **100**, 433 (2002).
[81] R. W. Godby, M. Schlüter, and L. J. Sham, Phys. Rev. B **36**, 6497 (1987).
[82] R. W. Godby, M. Schlüter, and L. J. Sham, Phys. Rev. B **37**, 10159 (1988).
[83] Z.-H. Yang, H. Peng, J. Sun, and J. P. Perdew, Phys. Rev. B **93**, 205205 (2016).
[84] F. Tran and P. Blaha, Phys. Rev. Lett. **102**, 226401 (2009).
[85] J. Heyd, G. E. Scuseria, and M. Ernzerhof, J. Chem. Phys. **118**, 8207 (2003).
[86] J. Heyd and G. E. Scuseria, J. Chem. Phys. **121**, 1187 (2004).
[87] J. Heyd, J. E. Peralta, G. E. Scuseria, and R. L. Martin, J. Chem. Phys. **123**, 174101 (2005).
[88] S. Jana and P. Samal, Phys. Chem. Chem. Phys. **20**, 8999 (2018).
[89] S. Jana, A. Patra, and P. Samal, J. Chem. Phys. **149**, 094105 (2018).
[90] S. Jana and P. Samal, Phys. Chem. Chem. Phys. **21**, 3002 (2019).
[91] K. Finzel and A. I. Baranov, Int. J. Quantum Chem. **117**, 40 (2016).
[92] O. Gritsenko, R. van Leeuwen, E. van Lenthe, and E. J. Baerends, Phys. Rev. A **51**, 1944 (1995).
[93] M. Kuisma, J. Ojanen, J. Enkovaara, and T. T. Rantala, Phys. Rev. B **82**, 115106 (2010).
[94] F. Tran, S. Ehsan, and P. Blaha, Phys. Rev. Mater. **2**, 023802 (2018).
[95] L. G. Ferreira, M. Marques, and L. K. Teles, Phys. Rev. B **78**, 125116 (2008).
[96] L. A. Constantin, E. Fabiano, and F. Della Sala, Phys. Rev. B **84**, 233103 (2011).
[97] A. D. Becke, J. Chem. Phys. **109**, 2092 (1998).
[98] A. D. Becke, J. Chem. Phys. **140**, 18A301 (2014).
[99] S. Śmiga, E. Fabiano, L. A. Constantin, and F. Della Sala, J. Chem. Phys. **146**, 064105 (2017).
[100] S. Śmiga, E. Fabiano, S. Laricchia, L. A. Constantin, and F. Della Sala, J. Chem. Phys. **142**, 154121 (2015).
[101] A. C. Cancio and J. J. Redd, Mol. Phys. **115**, 618 (2017).
[102] D. Mejia-Rodriguez and S. B. Trickey, Phys. Rev. A **96**, 052512 (2017).
[103] D. Mejia-Rodriguez and S. B. Trickey, Phys. Rev. B **98**, 115161 (2018).
[104] M. Brack, B. K. Jennings, and Y. H. Chu, Phys. Lett. B **65**, 1 (1976).
[105] C. H. Hodges, Can. J. Phys. **51**, 1428 (1973).
[106] E. Proynov, Z. Gan, and J. Kong, Chem. Phys. Lett. **455**, 103 (2008).
[107] M. Levy and J. P. Perdew, Phys. Rev. A **32**, 2010 (1985).
[108] P. Elliott and K. Burke, Can. J. Chem. **87**, 1485 (2009).
[109] P. Elliott, D. Lee, A. Cangi, and K. Burke, Phys. Rev. Lett. **100**, 256406 (2008).
[110] L. A. Constantin, J. C. Snyder, J. P. Perdew, and K. Burke, J. Chem Phys. **133**, 241103 (2010).
[111] E. Fabiano and L. A. Constantin, Phys. Rev. A **87**, 012511 (2013).
[112] J. P. Perdew, J. Tao, V. N. Staroverov, and G. E. Scuseria, J. Chem. Phys. **120**, 6898 (2004).
[113] J. M. Crowley, J. Tahir-Kheli, and W. A. Goddard, J. Phys. Chem. Lett. **7**, 1198 (2016).
[114] J. Lee, A. Seko, K. Shitara, K. Nakayama, and I. Tanaka, Phys. Rev. B **93**, 115104 (2016).
[115] A. M. Ganose and D. O. Scanlon, J. Mater. Chem. C **4**, 1467 (2016).
[116] M. J. Lucero, T. M. Henderson, and G. E. Scuseria, J. Phys.: Condens. Matter **24**, 145504 (2012).
[117] L. Schimka, J. Harl, and G. Kresse, J. Chem. Phys. **134**, 024116 (2011).
[118] S. Bernstorff and V. Saile, Opt. Commun. **58**, 181 (1986).
[119] D. Koller, P. Blaha, and F. Tran, J. Phys.: Condens. Matter **25**, 435503 (2013).
[120] J. H. Skone, M. Govoni, and G. Galli, Phys. Rev. B **89**, 195112 (2014).
[121] D. Groh, R. Pandey, M. B. Sahariah, E. Amzallag, I. Baraille, and M. Rérat, J. Phys. Chem. Solids **70**, 789 (2009).
[122] F. Tran and P. Blaha, J. Phys. Chem. A **121**, 3318 (2017).
[123] P. Blaha, K. Schwarz, G. K. H. Madsen, D. Kvasnicka, J. Luitz, R. Laskowski, F. Tran, and L. D. Marks, *WIEN2K, An Augmented Plane Wave + Local Orbitals Program for Calculating Crystal Properties* (Vienna University of Technology, Austria, 2018).
[124] H. Jiang, J. Chem. Phys. **134**, 204705 (2011).
[125] S. Tongay, J. Zhou, C. Ataca, K. Lo, T. S. Matthews, J. Li, J. C. Grossman, and J. Wu, Nano Lett. **12**, 5576 (2012).
[126] K. K. Kam and B. A. Parkinson, J. Phys. Chem. **86**, 463 (1982).
[127] A. Ghafari, A. Boochani, C. Janowitz, and R. Manzke, Phys. Rev. B **84**, 125205 (2011).
[128] G. Kresse and J. Hafner, Phys. Rev. B **47**, 558 (1993).
[129] G. Kresse and J. Furthmüller, Phys. Rev. B **54**, 11169 (1996).
[130] G. Kresse and D. Joubert, Phys. Rev. B **59**, 1758 (1999).
[131] G. Kresse and J. Furthmüller, Comput. Mater. Sci. **6**, 15 (1996).
[132] Z.-H. Cui, Y.-C. Wang, M.-Y. Zhang, X. Xu, and H. Jiang, J. Phys. Chem. Lett. **9**, 2338 (2018).
[133] Y.-S. Kim, M. Marsman, G. Kresse, F. Tran, and P. Blaha, Phys. Rev. B **82**, 205212 (2010).
[134] J. Klimeš and G. Kresse, J. Chem. Phys. **140**, 054516 (2014).
[135] N. Mounet, M. Gibertini, P. Schwaller, D. Campi, A. Merkys, A. Marrazzo, T. Sohier, I. E. Castelli, A. Cepellotti, G. Pizzi, *et al.*, Nat. Nanotechnol. **13**, 246 (2018).
[136] K. Berland and P. Hyldgaard, Phys. Rev. B **89**, 035412 (2014).
[137] T. Björkman, J. Chem. Phys. **141**, 074708 (2014).
[138] A. V. Terentjev, L. A. Constantin, and J. M. Pitarke, Phys. Rev. B **98**, 214108 (2018).
[139] H. Peng, Z.-H. Yang, J. P. Perdew, and J. Sun, Phys. Rev. X **6**, 041005 (2016).
[140] B. Traoré, G. Bouder, W. Lafargue-Dit-Hauret, X. Rocquefelte, C. Katan, F. Tran, and M. Kepenekian, Phys. Rev. B **99**, 035139 (2019).
[141] P. S. Svendsen and U. von Barth, Phys. Rev. B **54**, 17402 (1996).
[142] P. R. Antoniewicz and L. Kleinman, Phys. Rev. B **31**, 6779 (1985).
[143] R. Neumann, R. H. Nobes, and N. C. Handy, Mol. Phys. **87**, 1 (1996).